



Predicting gridded winter PM_{2.5} concentration in east of China

Zhicong Yin^{1,2,3}, Mingkeng Duan¹, Yuyan Li¹, Tianbao Xu¹, Huijun Wang^{1,2,3}

¹Key Laboratory of Meteorological Disaster, Ministry of Education / Joint International Research Laboratory of Climate and Environment Change (ILCEC) / Collaborative Innovation Center on Forecast and Evaluation of Meteorological Disasters (CIC-FEMD), Nanjing University of Information Science & Technology, Nanjing, 210044, China

²Southern Marine Science and Engineering Guangdong Laboratory (Zhuhai), Zhuhai, 519080, China

³Nansen-Zhu International Research Centre, Institute of Atmospheric Physics, Chinese Academy of Sciences, Beijing, 100029, China

Correspondence to: Zhicong Yin (yinzhc@nuist.edu.cn)

Abstract. Exposure to high levels of concentration of fine particle matters with diameter ≤ 2.5 μm (PM_{2.5}) can lead to great threats to human health in east of China. Air pollution control has greatly reduced the PM_{2.5} concentration and entered a crucial stage that required supports like fine seasonal prediction. In this study, we analysed the contributions of emission predictors and climate variability to seasonal prediction of PM_{2.5} concentration. The socioeconomic-PM_{2.5}, isolated by atmospheric chemical models, could well describe the gradual increasing trend of PM_{2.5} during the winters of 2001–2012 and the sharp decreasing trend since 2013. The preceding climate predictors have successfully simulated the interannual variability of winter PM_{2.5} concentration. Based on the year-to-year increment approach, a model for seasonal prediction of gridded winter PM_{2.5} concentration (10km \times 10km) in east of China was trained by integrating of emission and climate predictors. The area-averaged percentage of same sign was 81.8% (relative to the winters of 2001–2019) in the leave-one-out validation. In three densely populated and heavily polluted regions, the correlation coefficients were 0.93 (North China), 0.95 (Yangtze River Delta) and 0.88 (Pearl River Delta) during 2001–2019 and the root-mean-square errors were 6.5, 4.1 and 4.6 $\mu\text{g}/\text{m}^3$. More important, the significant decrease in PM_{2.5} concentration, resulted from implementation of strict emission control measures in recent years, was also reproduced. In the recycling independent tests, the prediction model developed in this study also maintained high accuracy and robustness. Furthermore, the accurate gridded PM_{2.5} prediction had the potential to support air pollution control on regional and city scales.



30 1 Introduction

31 Exposure to fine particle matters with diameter $\leq 2.5 \mu\text{m}$ ($\text{PM}_{2.5}$) can lead to severe respiratory and cardiovascular
32 diseases (Cohen et al., 2017) and even directly induces DNA damages (Wu et al., 2017). According to the newly
33 recommended air quality guidelines, the level of annual mean $\text{PM}_{2.5} > 5 \mu\text{g}/\text{m}^3$ has the potential to threat human health
34 (World Health Organization, 2021). In 2020, the average $\text{PM}_{2.5}$ concentration in cities of China was $33 \mu\text{g}/\text{m}^3$, although the
35 implementation of strict air quality control measures substantially reduced the emission of primary pollutants (Zhang et al.,
36 2022). The changes in the emission of air pollutants also resulted in the shift of winter $\text{PM}_{2.5}$ trend in east of China, that is,
37 the winter $\text{PM}_{2.5}$ concentration gradually increased during 2000–2012 but has been decreasing since 2013 (Figure 1a).
38 Evident interannual variation was also be found in the changes of $\text{PM}_{2.5}$ concentration in winter, which was largely attributed
39 to climate variability (Yin et al., 2020a, 2020b). Given the severe impact of $\text{PM}_{2.5}$ pollution and yearly plan of control action,
40 it is meaningful and urgent to develop prediction models to forecast $\text{PM}_{2.5}$ concentration 1~3 months in advance.
41 Furthermore, the predicting results should have high resolution to provide valuable information on the regional and city
42 levels.

43 To accurately predict climate anomalies is still a real challenge, while predicting air pollution on seasonal scale is much
44 harder than predicting routine meteorological elements (Wang et al., 2021). In general, the methods of climate prediction
45 included numerical climate models and statistical approaches. Despite the great advances in atmospheric chemical models in
46 recent years, most of these models were not designed for real-time operation of seasonal predictions and lacked the coupling
47 of the atmospheric chemical composition and the entire earth system (An et al., 2018). Additionally, statistical prediction of
48 winter $\text{PM}_{2.5}$ concentration was limited by the short sequences of observed atmospheric composition, because broad
49 observations only started in 2014 in China. The gray prediction model performed well in dealing with small sample data and
50 thus was used to forecast $\text{PM}_{2.5}$ concentration (Wang and Du, 2021; Wu et al., 2019; Xiong et al., 2019). Considering the
51 strong control measures implemented to improve air quality, the buffer operators can be added to the discrete gray prediction
52 model to reduce deviations (Dun et al., 2020). These mathematical models showed certain predictive skills, but lacked of
53 underlying physical mechanisms and long-standing robustness.

54 Many previous studies employed the long-term observed visibility, air humidity and weather phenomena to reconstruct
55 data of haze (Xu et al., 2016; Zou et al., 2017; He et al., 2019; Yin et al., 2020b). The change in winter haze days consists of
56 long-term trend and interannual-decadal variations. The long-term trend of haze was mainly determined by human activities
57 (i.e., primary pollutants emission and climate change), while its interannual-decadal variations had close relationships with
58 climate variability (Yin et al., 2020b; Geng et al., 2021a). Besides analysis of climate mechanisms, the number of haze days
59 was also used as a proxy-predictand of $\text{PM}_{2.5}$ pollution. Taking advantage of the memory effect in slow-varying climate
60 forcings (e.g., sea surface temperature and sea ice), the number of haze days was successfully predicted in North China (Yin
61 and Wang 2016; Yin et al., 2017), Yangtze River Delta (Dong et al., 2021) and Fenwei Plain (Zhao et al., 2021). Chang et al.
62 (2021) used regional stratospheric warming over northeastern Asia in November to predict haze pollution in the Sichuan



63 Basin in 5–7 weeks. Information from the preceding autumn El Niño was also extracted to predict winter haze days in South
64 China (Cheng et al., 2019) and aerosol optical depth over northern India (Gao et al., 2019). In most of these studies, the
65 predictand is area-averaged number of haze days, which was a bit different from PM_{2.5} concentration in use and fine spatial
66 information was missing.

67 The Tracking Air Pollution (TAP) database combines information from ground observations, satellite retrievals,
68 emission inventories and chemical transport model simulations based on data fusion. A full-coverage PM_{2.5} reanalysis
69 dataset with a spatial resolution of 10km×10km from 2000 until present has been released (Geng et al., 2021b). It becomes
70 feasible to develop statistical prediction model of PM_{2.5} concentration based on this long-range dataset. Furthermore, as
71 reviewed by Yin et al., (2022), the predictability of winter haze decreased during 2014–2020, which was mainly attributed to
72 the disturbances from super-strict emissions reduction in China. Rapid changes in human activities and changes in climate
73 anomalies both should be considered and included in PM_{2.5} prediction models. This is the major motivation of the present
74 study to build a climate-emission hybrid model for the prediction of gridded PM_{2.5} concentration in east of China. The
75 findings of this study have enormous potentials to support fine designs and implements of air pollution control in advance.

76 **2 Datasets and method**

77 **2.1 Data**

78 The monthly sea ice concentration (SI) and sea surface temperature (SST) dataset, with a spatial resolution of 1°×1°,
79 were provided by the Met Office Hadley Centre (Rayner et al. 2003, <https://www.metoffice.gov.uk/hadobs/hadisst/>).
80 Monthly soil moisture (Soilw), snow depth (SD), geopotential height at 500hPa (Z500) and 850hPa (Z850), sea level
81 pressure (SLP) and 10m wind were extracted from the fifth generation reanalysis product (ERA5) produced by the European
82 Center for Medium Range Weather Forecasts (Hersbach et al. 2020,
83 <https://cds.climate.copernicus.eu/#!/search?text=ERA5&type=dataset>). Annual emissions of ammonia, nitrogen oxide, BOC,
84 primary PM_{2.5}, and sulfur dioxide in China were derived from the MEIC model (<http://www.meicmodel.org/>; Li et al., 2017).

85 Hourly site-observed PM_{2.5} concentration during 2014–2020 were also employed in the present study
86 (<https://www.aqistudy.cn/historydata/>). The long-term and high-resolution TAP PM_{2.5} concentration dataset during 2000-
87 2020 can be downloaded from <http://tapdata.org> (Geng et al. 2021b). The PM_{2.5} reanalysis data were used as training data as
88 well as test data in the construction of the prediction model, and the observed PM_{2.5} concentration were also applied to verify
89 the prediction skill of the model.

90 **2.2 Isolation of socioeconomic-PM_{2.5}**

91 We employed the simulated annual-mean PM_{2.5} concentrations that exclude the meteorological contributions to
92 represent the impacts of anthropogenic emissions. Compared with direct use of emission inventory of primary pollutants, the



93 isolated socioeconomic-PM_{2.5} (SE-PM_{2.5}) involved both results of emission changes and follow-up physical and chemical
94 reactions in the air. To remove the meteorological influences from the TAP PM_{2.5} data, we used chemical transport models
95 and emission inventories to separate the contributions from emission and meteorology changes. Following the approach
96 proposed by Xiao et al. (2021), we used a ‘fix emission’ scenario to quantify the impacts of interannual meteorological
97 variation on PM_{2.5} concentration in Community Multiscale Air Quality (CMAQ) model. Subsequently, a full simulation with
98 year-by-year emission and meteorology was completed. Differences between the ‘fix emission’ simulation and the full
99 simulation were considered to be PM_{2.5} concentrations driven by anthropogenic emissions. This data has been analyzed to
100 quantify relative influences of different drivers on PM_{2.5}-related deaths in China (Geng et al. 2021b).

101 2.3 Year-to-year increment prediction

102 The year-to-year increment approach is proposed to improve the skill of climate prediction (Wang et al., 2008), in
103 which the predicted object is not climate anomalies but is the difference between the current and the previous year (DY).
104 After adding the predicted DY to the observed predictand in the year before, the final predicted results were obtained. Based
105 on full use of observations in the previous year, the gradually changing trend and inter-decadal components can be well
106 reproduced. Anthropogenic-natural-forcing predictand could be represented by $Y = Y_S + Y_C$, where Y_S and Y_C denoted the
107 slowly varying socio-economic and climatic components, respectively. In the DY approach, which was expressed by:

$$108 \quad DY = Y_t - Y_{t-1} = (Y_{S_t} + Y_{C_t}) - (Y_{S_{t-1}} + Y_{C_{t-1}}) = (Y_{S_t} - Y_{S_{t-1}}) + (Y_{C_t} - Y_{C_{t-1}})$$

109 where the subscripts t and $t-1$ indicated the current and the previous years. Before 2013, the difference between
110 anthropogenic emissions in two adjacent years was small, Yin and Wang (2016) assumed $(Y_{S_t} - Y_{S_{t-1}}) \approx 0$ and proposed
111 that DY was mainly influenced by climate variability. However, due to significant reduction of anthropogenic emissions
112 after the implementation of China’s Air Pollution Prevention and Control Action Plan (Zhang and Geng, 2020), the
113 assumption of $(Y_{S_t} - Y_{S_{t-1}}) \approx 0$ was no longer completely valid. Therefore, it is meaningful to consider the information of
114 rapid emission changes and re-build the prediction model (Yin et al., 2022).

115 (1) Seasonal prediction model based on SE-PM_{2.5} (SP-SE): this prediction model unilaterally emphasized the impacts of
116 human activities and was trained by DY of SE-PM_{2.5} in each grid.

117 (2) Seasonal prediction model based on preceding climate variability (SP-CV): this prediction model was highly
118 focused on the impacts of climate condition and trained by DY of closely related climate factors.

119 (3) Seasonal prediction model based on both SE-PM_{2.5} and climate (SP-EC): the contributions of emissions and climate
120 factors are incorporated into one prediction model, i.e., combining the PM_{2.5} DY from SP-SE and SP-CV.

121 In the leave-one-out cross validation, root-mean-square error (RMSE), relative bias and correlation coefficient (CC)
122 were calculated. When discussing the CC after the detrending, the linear trend was removed by stages (i.e., winters of 2001-



123 2011 and 2012–2019). The percentage of the same sign (PSS; same sign means the mathematical sign of the fitted and
124 observed $PM_{2.5}$ anomalies was the same) was also computed.

125 **3 Relative contributions of emission and climate predictors**

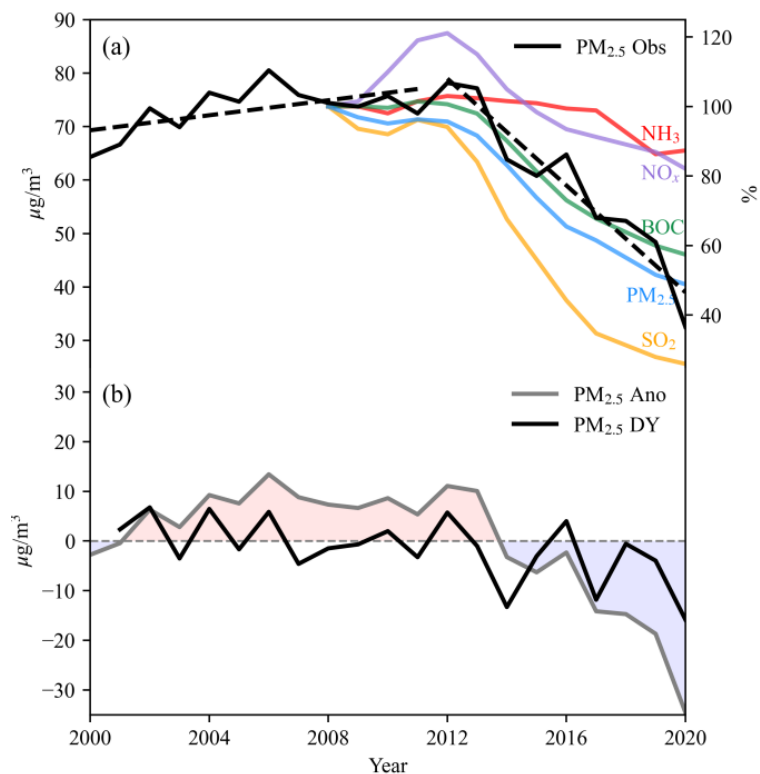
126 **3.1 Roles of emission**

127 Human activities are the major source of haze pollution in east of China (Zhang and Geng, 2020), which implies that a
128 large proportion of $PM_{2.5}$ concentration is predictable. Particularly, the large reduction of anthropogenic emissions since
129 2013 determined the decreasing trend of winter $PM_{2.5}$ concentration (Figure 1a). As aforementioned, the socioeconomic-
130 $PM_{2.5}$ (i.e., SE- $PM_{2.5}$) isolated by CMAQ could well reflect the impacts of human activities and was a potentially effective
131 predictor for seasonal prediction of $PM_{2.5}$ concentration. As expected, the one-variable linear regression model based on
132 anomalies of SE- $PM_{2.5}$ successfully reproduced different slopes of trend during 2001–2007, 2008–2013 and 2014–2019, but
133 the predicted $PM_{2.5}$ concentration varied too smoothly (Figure S1a). Furthermore, the quantities were underestimated when
134 observed $PM_{2.5}$ concentration increased and overestimated when $PM_{2.5}$ concentration rapidly decreased. To eliminate the
135 influence of trend shift, we calculated DY of $PM_{2.5}$ and SE- $PM_{2.5}$. Compared with its anomalies, $PM_{2.5}$ DY did not show
136 significant trend but displayed regularly oscillating characteristic (Figure 1b), and its predictability was much better (Wang
137 et al., 2008). The SP-SE model was trained by DY of SE- $PM_{2.5}$ in each grid to predict $PM_{2.5}$ DY. After adding the predicted
138 $PM_{2.5}$ DY to observed $PM_{2.5}$ in the previous year, the final $PM_{2.5}$ concentration was obtained. The CC between predicted and
139 observed $PM_{2.5}$ was 0.87 during 2001–2019 in the east of China. The underestimated (2001–2007) and overestimated (2014–
140 2019) values in Figure S1a were largely corrected and interannual variation also appeared in the results of SP-SE prediction
141 (Figure S1b). The staged trends from the SP-SE model almost overlapped with the observed trends, indicating the model
142 performed well in capturing the changes of trend (Figure S2).

143 North China (NC; 34–42°N, 114–120°E), the Yangtze River Delta (YRD; 27–34°N, 117–122°E) and the Pearl River
144 Delta (PRD; 21.5–25°N, 112–116°E) are three regions that have been experiencing severe $PM_{2.5}$ pollution (Yin et al., 2015).
145 Thus, the performance of the SP-SE model in NC, the YRD and the PRD were validated separately (Table 1, Figure 2 a-c).
146 The RMSEs were 12.2, 6.2 and 6.8 $\mu\text{g}/\text{m}^3$ in NC, the YRD and the PRD, respectively (Table 1). Larger RMSE in NC did not
147 indicate the SP-SE model performs worse in NC than in the YRD and the PRD, because the mean value of $PM_{2.5}$
148 concentration was the highest in NC. The relative bias (absolute bias/mean) in NC was 8.5%, which was smaller than that in
149 the PRD (12.9%). Consistent with its performance in east of China, the SP-SE model also well reproduced the staged trends
150 in NC, the YRD and the PRD (Figure 2 a-c). However, when the linear trend was removed, the CC between predicted and
151 observed $PM_{2.5}$ significantly decreases in all the three $PM_{2.5}$ -polluted regions (NC: from 0.78 to –0.13; YRD: from 0.88 to –
152 0.28; PRD: from 0.74 to 0.16). That is, the prediction model trained by the socioeconomic- $PM_{2.5}$ could well predict the



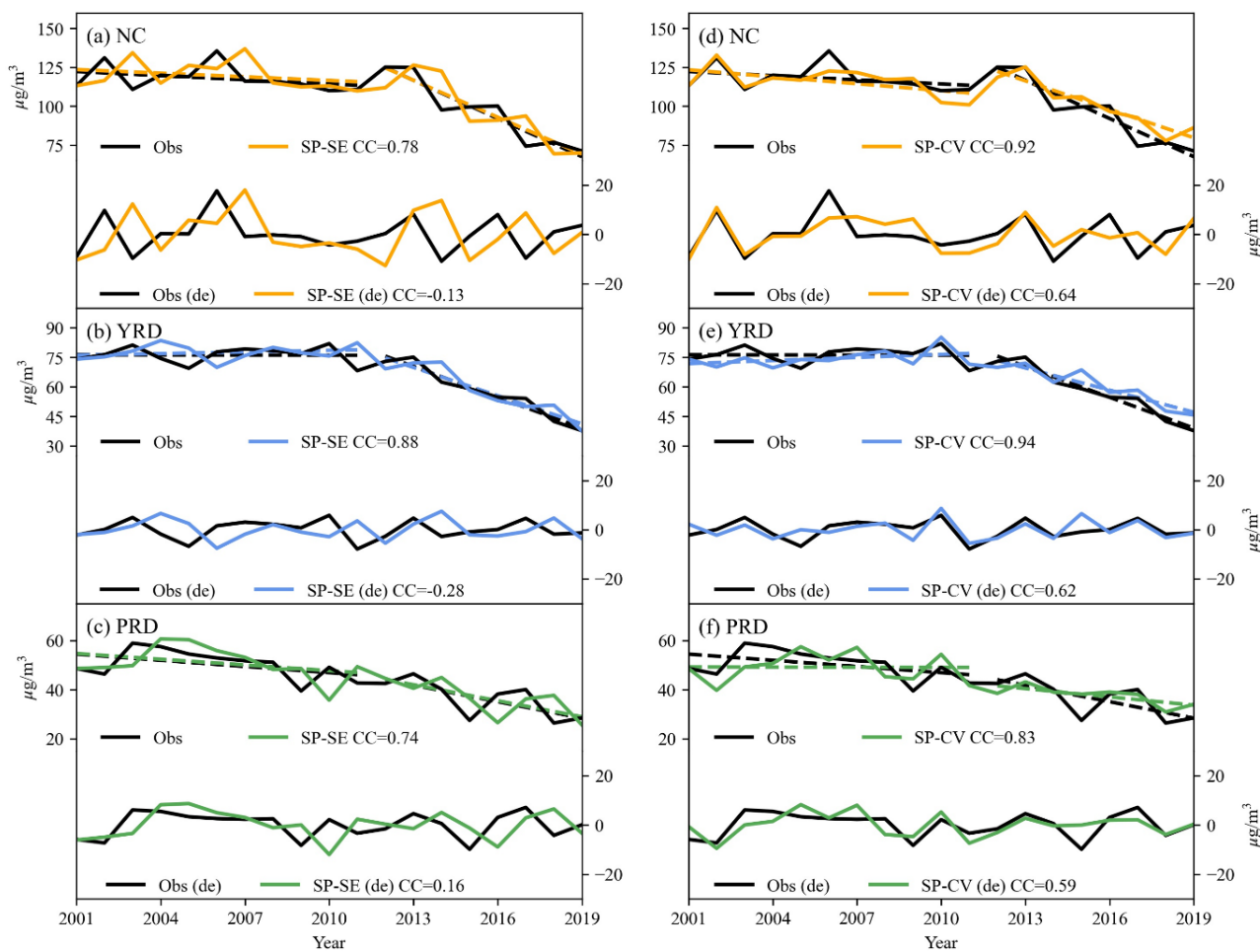
153 values and staged linear trends. However, it certainly had no ability to simulate the interannual variability of $PM_{2.5}$
 154 concentration.



155
 156 **Figure 1: Variation in (a) winter $PM_{2.5}$ concentration (black; unit: $\mu\text{g}/\text{m}^3$), (b) $PM_{2.5}$ anomalies (gray; compared to the mean of**
 157 **2000–2020; unit: $\mu\text{g}/\text{m}^3$) and $PM_{2.5}$ DY (black; unit: $\mu\text{g}/\text{m}^3$). Color lines in panel (a) indicate relative variations in annual emissions**
 158 **(compared to that in 2008, unit: %) of ammonia (NH_3 ; red), nitrogen oxide (NO_x ; purple), BOC (green), $PM_{2.5}$ (blue), and sulfur**
 159 **dioxide (SO_2 ; yellow) in east of China. The black dashed line in panel (a) indicates the linear trend of $PM_{2.5}$ concentration.**

160
 161 **Table 1: The leave-one-out validated root-mean square errors (RMSE), relative biases (absolute bias mean; %) and percentages of**
 162 **same sign (PSS) for three statistical models.**

| | RMSE ($\mu\text{g}/\text{m}^3$) | | | Relative Bias (%) | | |
|-------|-----------------------------------|-----|-----|-------------------|-----|------|
| | NC | YRD | PRD | NC | YRD | PRD |
| SP-SE | 12.2 | 6.2 | 6.8 | 8.5 | 6.9 | 12.9 |
| SP-CV | 7.6 | 4.7 | 5.2 | 5.2 | 5.9 | 9.7 |
| SP-CE | 6.5 | 4.1 | 4.6 | 4.8 | 5.1 | 8.5 |



167

168 **Figure 2: Variations in reanalysis (black) and SP-SE predicted winter PM_{2.5} concentration in (a) NC (orange), (b) the YRD (blue),**
169 **and (c) the PRD (green) from 2001 to 2019 before (upper) and after (lower) detrending. The predicted PM_{2.5} is dependent on the**
170 **leave-one-out validation. (d-f) are the same as (a-c), but for SP-CV.**

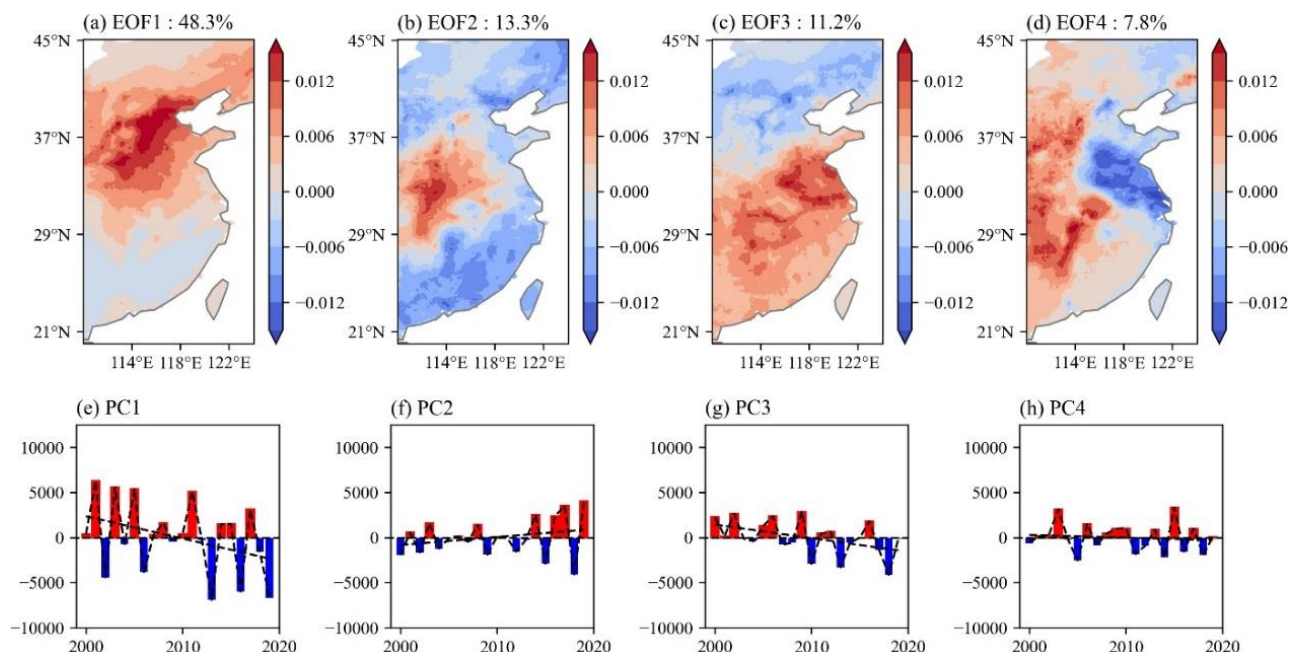
171 3.2 Impacts of climate variability

172 Decomposition and prediction of dominant modes of climate conditions were applied in short-term prediction of
173 precipitation (Huang et al., 2022) and surface air temperature (Hsu et al., 2020) in east of China. In this study, we decompose
174 the first four leading modes of PM_{2.5} DY during 2001-2019 (accumulated variance contribution=80.5%) produced by
175 Empirical Orthogonal Function (EOF) analysis, built prediction model for each principal component respectively, recalculate
176 the predicted PM_{2.5} DY by projecting the predicted PCs onto the observed EOF spatial patterns, and finally added the
177 predicted PM_{2.5} DY to the observation in previous year to finish the development of SP-CV (Figure S3, Table S1). The
178 interannual-decadal variation in haze pollution could be well explained by meteorological condition and preceding climate



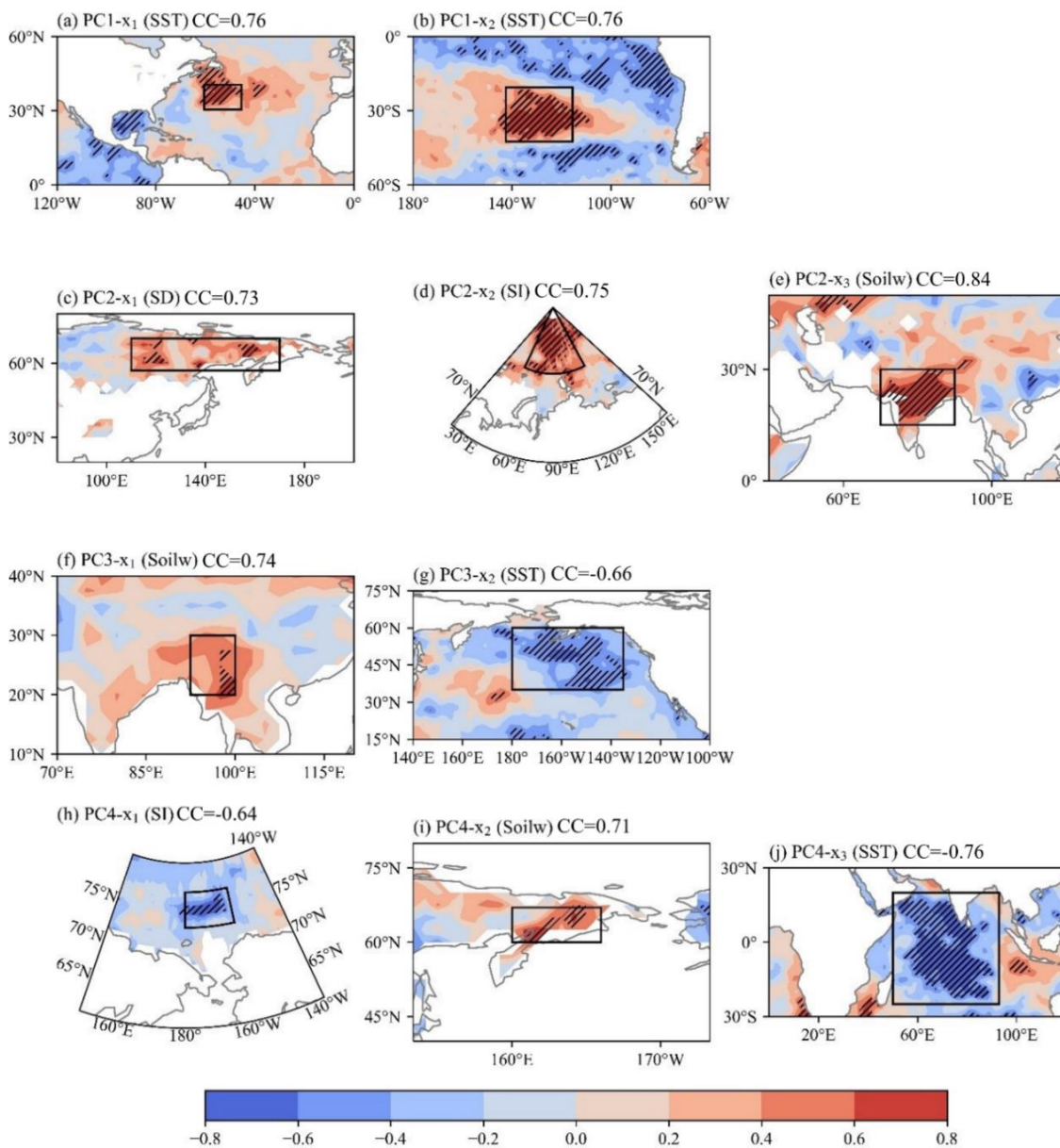
179 forcings (Yin et al., 2020b) such as the Arctic sea ice extent (Wang et al., 2015; Yin et al., 2019), Eurasia snow (Zou et al.,
180 2017) and soil moisture (Yin and Wang 2018), SST in the Pacific (Yin and Wang 2016; He et al., 2019) and Atlantic (Yin
181 and Zhang 2020a). Prediction signals from these climate anomalies could be observed before winter and owned specific
182 physical implications.

183 The first EOF mode of $PM_{2.5}$ DY illustrated heavily haze-polluted status in NC (Figure 3a, e). According to the
184 correlation analysis, the September SST DY in the Southwest Pacific (CC with PC1=0.76; Figure 4a) and October SST DY
185 in the Sargasso Sea (CC=0.76; Figure 4b) were selected to be the two predictors for PC1 of $PM_{2.5}$ DY (Table S1). Both of
186 the predictors had close relationships with dipole pattern of Eurasian anti-cyclonic and Northeast Asian cyclonic circulations
187 (Figure S4b, c), which was identical to those associated with PC1 (Figure S4a) and could induce cold air from high latitude
188 to deviate from NC. The second EOF mode indicated a tripole pattern with centers located in the Inner Mongolia, the Fenwei
189 Plain and South China, respectively (Figure 3b, f). The Fenwei Plain was highly polluted and gained a great attention in
190 recent years, while the other two centers have relatively better air quality (Zhao et al., 2021). The October snow depth DY in
191 eastern Siberia (CC with PC2=0.73; Figure 4c), October sea ice DY in the north to Barents Sea (CC=0.75; Figure 4d) and
192 September-October soil moisture DY in the Indian Peninsula (CC=0.84; Figure 4e) were considered in the prediction model
193 (Table S1). The predictors possibly induced atmospheric responses in winter (Figure S4 e-g) that were similar to PC2
194 (Figure S4 d). The anti-cyclonic anomaly over the Fenwei Plain restricted horizontal and vertical dispersion of haze particles
195 (Zhong et al., 2019).



196

197 **Figure 3: Spatial patterns (a–d) and corresponding PCs (e–h) of the first four EOF modes for winter $PM_{2.5}$ DY in east of China**
198 **during 2000–2020. The variance accounted for by each EOF mode is given in the panel.**



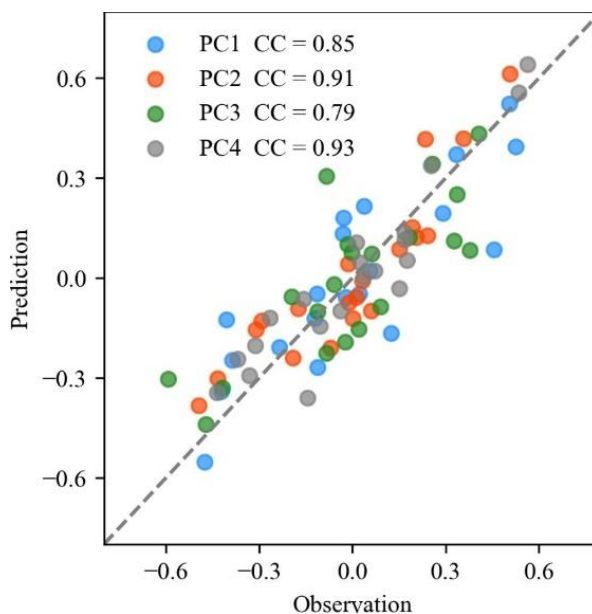
199

200 **Figure 4:** CCs between climate predictors and (a-b) PC1, (c-e) PC2, (g-f) PC3, (h-j) PC4 from 2000 to 2020. The predictors for PC1
 201 are (a) September SST over the South Pacific Ocean and (b) October SST over the Sargasso Sea. The predictors for PC2 are
 202 (c) October Sd over eastern Siberia, (d) October SI over the Kara Sea and (e) September-October Soilw over the Indian Peninsula.
 203 The predictors for PC3 are (f) October Soilw over the Indo-China Peninsula and (g) June-August SST over the Gulf of Alaska.
 204 The predictors for PC4 are (h) October SI over the Chukchi Sea, (i) October soil moisture over the Kamchatka Peninsula and (j)
 205 August-September SST over the Arabian Sea and the Bay of Bengal. The slashes indicate CCs exceeding the 95% confidence level.
 206 The black boxes indicate the regions over which the predictors are calculated.



207 The third EOF mode of $PM_{2.5}$ DY showed a ‘north-south’ dipole pattern (Figure 3c, g). The variations of $PM_{2.5}$ DY in
208 Huanghai and the YRD accounted for a large proportion. The October soil moisture DY in the Indo-China Peninsula (CC
209 with PC3=0.74; Figure 4f) and June-August SST DY in the Gulf of Alaska (CC=-0.66; Figure 4g) were selected to build
210 prediction model of PC3 (Table S1). The anomalous atmospheric circulation associated with PC3 and its predictors could
211 enhance cold air invasion to NC but prevented the cold air from moving further south (Figure S4 h-j). A statistical model
212 (Table S1) was also developed to predict the ‘East-West’ dipole shown in the fourth EOF mode (Figure 3d, h) based on
213 October sea ice DY in the Chukchi Sea (CC=-0.64; Figure 4h), October soil moisture DY in the Kamchatka peninsula
214 (CC=0.71; Figure 4i) and August-September SST DY in the Arabian Sea (CC=-0.76; Figure 4j). The atmospheric anomalies
215 in the lower troposphere and near surface, which were associated with the above predictors and PC4, also had similar
216 impacts on haze pollution (Figure S4 k-n).

217 As shown in Figure 5, multiple linear regression model demonstrated good performance in simulating the variation in
218 each PC. The CCs between observed and predicted 1st-4th PCs were 0.85, 0.91, 0.79 and 0.93, respectively, all of which
219 were above the 99% confidence level, indicating that the model successfully reproduced each individual EOF mode.
220 Meanwhile, the yearly increment approach had the ability to address trend and its changes that were not obviously
221 mutational (Yin and Wang 2016). The CC between observed and predicted $PM_{2.5}$ concentrations before (after) detrending by
222 stages was 0.92 (0.64) in NC, 0.94 (0.62) in the YRD and 0.83 (0.59) in the PRD in the leave-one out validation (Figure 2 d-
223 f). Thus, the SP-CV model well simulated both the trend and the interannual variation of $PM_{2.5}$ concentration in the east of
224 China. In addition, the RMSEs in NC, the YRD and the PRD were 7.6, 4.7 and 5.3 and the relative biases were 5.2%, 5.2%
225 and 5.9%, respectively (Table 1), all of which were obviously smaller than those of SP-SE. The PSS, which is an important
226 indicator of climate prediction, was also evaluated relative to the winters of 2001–2019. The area-averaged PSS from SP-CV
227 was 80.1% in east of China, which was 8.1% higher than that from SP-SE (Figure 6). Although the SP-CV model performed
228 better than the SP-SE, especially that it could capture the sharp downward trend after 2013 in NC and YRD, the RMSEs of
229 the SP-CV simulations for the period 2015-2019 increased up to 11.1, 6.4 and 5.8 $\mu\text{g}/\text{m}^3$ in NC, the YRD and the PRD
230 compared to that of the SP-SE simulations. Obvious positive biases were found in the predictions of $PM_{2.5}$ concentration
231 after 2014 (Figure 2 d-f) because the SP-CV model was short of information about the super-strict emission regulations
232 (Figure S2). Based on different levels of haze pollution, various degrees of air pollution control were carried out in NC, the
233 YRD and the PRD (Zhang and Geng, 2020). In NC, where anthropogenic emissions were most prominently restricted, the
234 predicted biases were also the largest (Figure 2d). The predicted biases were the smallest in the PRD, while that in the YRD
235 were in-between. These results were consistent with different intensities of pollution control in the three regions (Figure 2e,
236 f), which further indicated the importance to fully take into account the impacts of climate variability and anthropogenic
237 emissions.



238

239 **Figure 5: Scatter plots of observed (x axis) and predicted (y axis) PC1 (blue), PC2 (red), PC3 (green) and PC4 (gray) from 2000 to**
240 **2020. The predicted PCs are dependent on the leave-one-cross validation.**

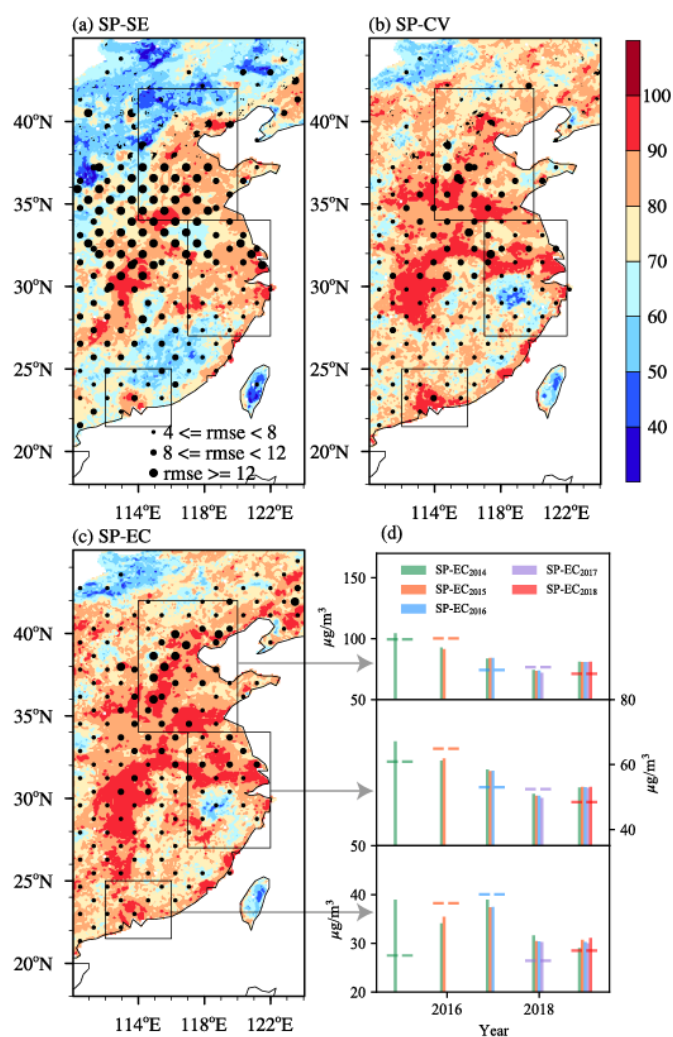
241 **4 PM_{2.5} prediction with integrated factors**

242 As aforementioned, the SP-SE model trained by the SE-PM_{2.5} DY considered the impacts of emission changes one-
243 sidedly and could well simulate the values and staged trends. However, it completely failed to reproduce the interannual
244 variation of winter PM_{2.5} concentration in east of China (Figure 2 a-c). Differently, the predictors of climate variability could
245 introduce the interannual variation of winter PM_{2.5} and the yearly increment approach had the ability to bring in the slow
246 trend. The SP-CV model successfully predicted most of the trend and interannual variation in PM_{2.5} concentration (Figure 2
247 d-f) but underestimated the sharp decreasing trend (Figure S2), which led to positive forecast biases after 2013 (Figure 2d-f).

248 To fully contain predictive signals of human activities and climate anomalies, the predicted PM_{2.5} DY from SP-SE and
249 SP-CV model for the current year were added up and the sum was added to PM_{2.5} observations in the previous year to
250 develop the final prediction model, i.e., the SP-EC model. As expected, the performance of SP-EC model was better than
251 that of both SP-SE and SP-CV models. Area-averaged PSS was 81.8% in east of China (Figure 6). The CC between
252 observed and SP-EC-predicted PM_{2.5} concentrations before (after) detrending was 0.96 (0.78) in east of China; the RMSE
253 was 2.57 $\mu\text{g}/\text{m}^3$, which was 47% (33%) smaller than the RMSE of SP-SE (SP-CV) in the leave-one out validation. That is,
254 the trend simulated by the SP-EC model almost overlapped with the trend of observations (similar to results of SP-SE) and
255 the interannual variation was also reproduced (similar to results of SP-CV). The CCs between observed and SP-EC-predicted
256 PM_{2.5} concentrations before (after) detrending were 0.93 (0.68) in NC, 0.95 (0.44) in the YRD and 0.88 (0.66) in the PRD.

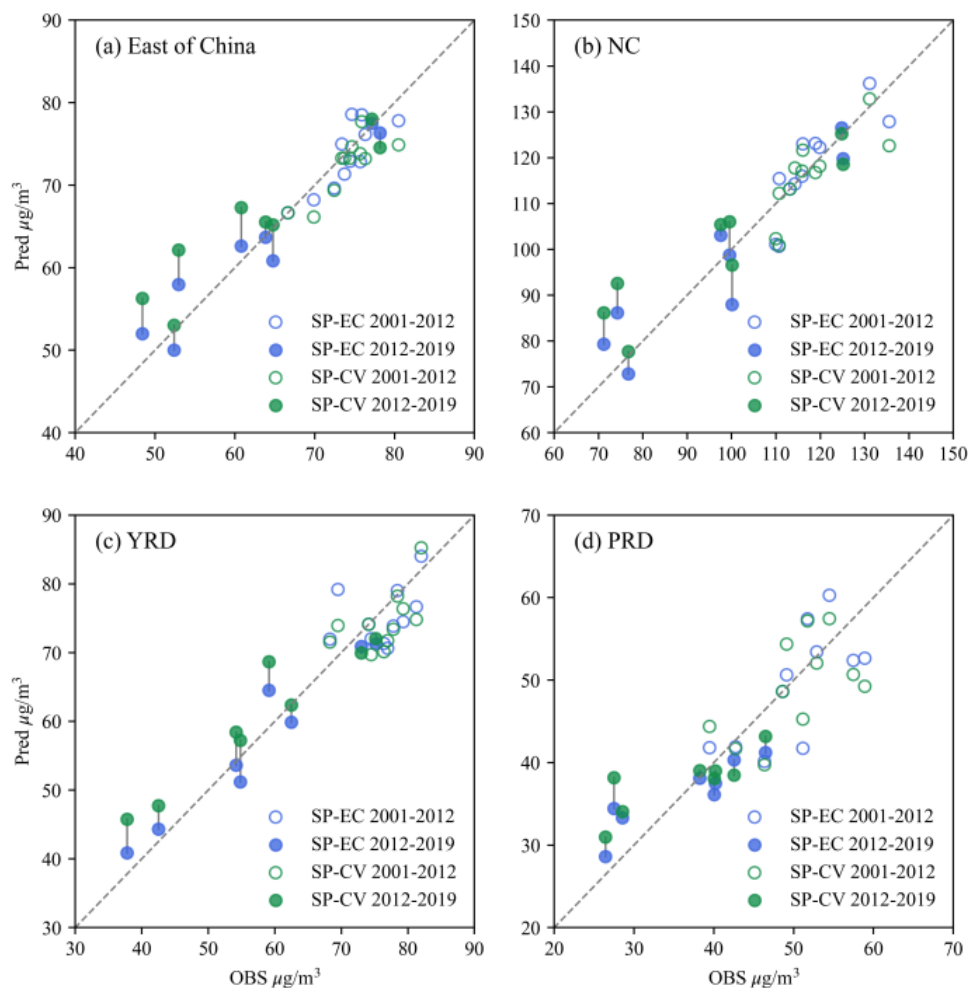


257 The RMSEs were 6.5 in NC, 4.1 in YRD and 4.6 $\mu\text{g}/\text{m}^3$ in PRD, which were 46.7% (14.5%), 33.9% (12.8%) and 32.4%
258 (11.5%) smaller than that of SP-SE (SP-CV), indicating greater improvements in NC than in the other two regions (Table 1).
259 According to the relative biases, the SP-EC model also demonstrated a better skill in NC (4.8%) than that in the YRD (5.1%)
260 and the PRD (8.5%) in the leave-one out validation. As shown in Figure 7, the decreases in $\text{PM}_{2.5}$ resulted from the
261 implementation of strict emission control measures in recent years were also reproduced by the SP-EC model. The evident
262 and positive biases in the SP-CV results were largely corrected in east of China, NC, the YRD and the PRD (Figure 7).



263

264 **Figure 6: Distributions of PSS (shadings) and RMSE (dots) from (a) SP-SE, (b) SP-CV, and (c) SP-EC. The boxes represent NC,**
265 **the YRD and the PRD respectively, and the arrows point to the SP-EC predicted $\text{PM}_{2.5}$ in recycling independent tests (bars) and**
266 **observations (dashed lines) corresponding to the area. The subscript in the legend of panel (d) indicates the model trained from**
267 **2000 to this year, and the $\text{PM}_{2.5}$ from the next year to 2019 are independently predicted.**



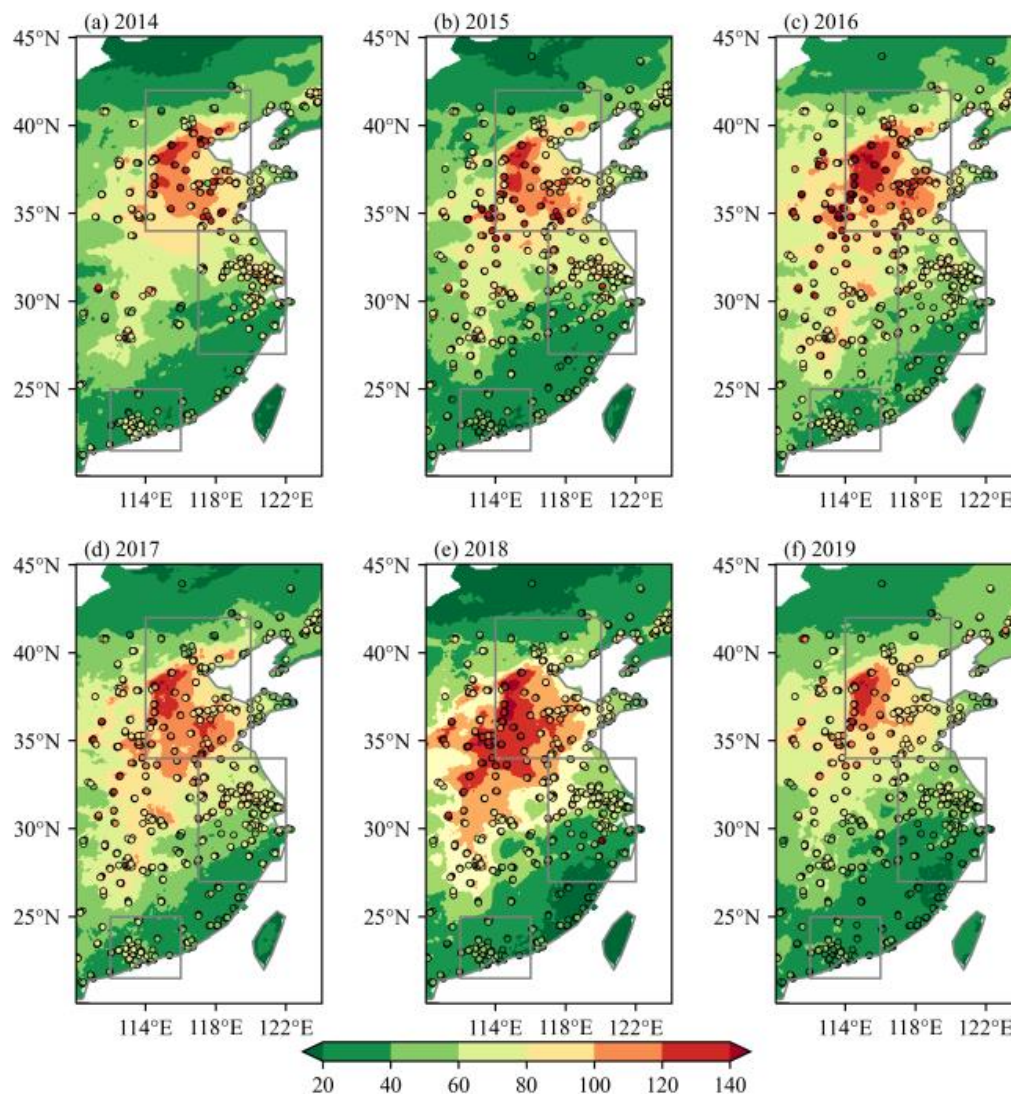
268

269 **Figure 7: Scatter plots of the reanalysis (x axis) and predictions of (y axis) $PM_{2.5}$ concentration by SP-CV (green) and SP-EC (blue)**
270 **in (a) east of China, (b) NC, (c) the YRD and (d) the PRD. The points during 2012–2019 are filled and the short lines between SP-**
271 **CV and SP-EC points indicate the calibrations.**

272 High spatial resolution was one of the advantages of the seasonal prediction model developed in this study. That is, the
273 SP-EC model could predict winter $PM_{2.5}$ concentration at each $10\text{km} \times 10\text{km}$ grid in east of China. When only considering
274 emission predictors (i.e., SP-SE), $RMSEs > 12 \mu\text{g}/\text{m}^3$ were found in middle part of the study region and the PSS was lower
275 than 60% in South China and the Inner Mongolia (Figure 6a). When only considering climate predictors (i.e., SP-CV),
276 $RMSEs > 12 \mu\text{g}/\text{m}^3$ existed in Beijing and its surrounding areas and PSS significantly increased compared to the result of SP-
277 SE (Figure 6b). When integrating both of the emission predictors and climate predictors (i.e., SP-EC), the RMSE in each
278 grid further decreased and the PSS also increased (Figure 6c). In middle part of the study region, the PSS was higher than
279 80%. In view of gaps between site observations and model simulations, the SP-EC-predicted $PM_{2.5}$ concentrations were



280 compared with site observations (Figure 8). NC was the most severely polluted area and the SP-EC model could capture the
281 $PM_{2.5}$ values and interannual differences. Particularly, the SP-EC model reproducee the sudden rebound of $PM_{2.5}$ pollution in
282 2018 (Figure 8e) that was mainly resulted from climate anomalies (Yin and Zhang 2020a). However, the model failed to
283 well predict the evident $PM_{2.5}$ drops in east of China (Figure 8f) caused by COVID-19 quarantines (Yin et al., 2021).



284

285 **Figure 8: SP-EC predicted (shading) and site-observed (scatter) $PM_{2.5}$ concentrations in (a) 2014, (b) 2015, (c) 2016, (d) 2017, (e)**
286 **2018 and (f) 2019. The boxes represent NC, the YRD and the PRD respectively.**

287 Due to the limitation of short sequence of data, recycling independent tests (RIT) were designed to further verify the
288 performance of the SP-EC model. In the RIT predictions, the prediction model was trained by samples from 2001 to the
289 expiration year of training data and the $PM_{2.5}$ anomalies from the next year to 2019 were independently predicted. For



290 example, the prediction model trained by the data from 2001 to 2014 can produce independent predictions from 2015 to
291 2019. The expiration year of the training data moved forward from 2015 to 2019, so there were 15 independent predictions.
292 The $PM_{2.5}$ concentration was independently predicted 5 times for 2019, 4 times for 2018, and so on. The PSS of $PM_{2.5}$
293 anomalies was 100%, not only relative to winters of 2001–2019 but also 2015–2019, indicating a high accuracy of prediction
294 in east of China. The predicted values for each year did not vary much (Figure 6d), indicating a high reliability and
295 robustness of the model. For example, when the SP-EC model was trained by the samples only from 2000 to 2014, the
296 predicted $PM_{2.5}$ anomalies for 2018 and 2019 were also close to the results of leave-one-out validations and the
297 measurements.

298 **5 Conclusions and discussion**

299 The change of haze pollution consisted of long-term trend, interannual-decadal variations, synoptic disturbances and so
300 on. Seasonal prediction was focused on predicting long-term trend and interannual-decadal variations 1~3 months in advance
301 (Wang et al., 2021). Because of the limitation of short observational period, many previous studies employed the number of
302 haze days as proxy of $PM_{2.5}$ pollution to build statistical prediction model (Yin and Wang 2016; Yin et al., 2017; Dong et al.,
303 2021; Zhao et al., 2021; Chang et al., 2021). Since 2020, several high-resolution $PM_{2.5}$ reanalysis datasets have been
304 successively released, which greatly increased the possibility for direct seasonal prediction of $PM_{2.5}$ concentration that is
305 more familiar to decision makers and the public (Yin et al., 2021).

306 In this study, two seasonal prediction models were separately trained by emission factor (i.e., SP-SE) or preceding
307 climate predictors (i.e., SP-CV) to discuss their relative contributions. The SP-SE model could simulate the slow rising trend
308 of $PM_{2.5}$ concentration before 2012 and the strong downward trend after 2012. However, it was incapable of importing the
309 interannual component. The SP-CV model benefited from the year-to-year increment approach and could introduce a large
310 portion of the linear trend except the sharp decrease of winter $PM_{2.5}$ concentration from 2013. Furthermore, the SP-CV
311 model performed well in predicting the obvious interannual variation of $PM_{2.5}$ concentration. We integrated the emission and
312 climate factors to establish the final prediction model (i.e., SP-EC), which could well reproduce both the trend and the
313 interannual variation of $PM_{2.5}$ concentration. The area-averaged PSS was 81.8% in east of China and CC between observed
314 and predicted $PM_{2.5}$ concentrations before (after) the detrending was 0.96 (0.78). The RMSEs were 6.5 in NC, 4.1 in the
315 YRD and 4.6 $\mu\text{g}/\text{m}^3$ in the PRD, which were 46.7% (14.5%), 33.9% (12.8%) and 32.4% (11.5%) smaller than that the results
316 of SP-SE (SP-CV). Due to the implementation of the super-strict emission control measures, the air quality has been
317 substantially improved and this improvement was also perfectly predicted by the SP-EC model. During recycling
318 independent tests, the PSS of $PM_{2.5}$ anomalies was 100%, demonstrating high accuracy and robustness. The high-resolution
319 $PM_{2.5}$ prediction could provide scientific supports for air pollution control at the regional and city levels.



320 This study mainly focused on the development of seasonal prediction model. Although the SP-EC model was proved to
321 be skilled, the underlying physical mechanisms of climate predictors were not sufficiently explained and needed further in-
322 deep studies. Furthermore, although the SP-EC model had high spatial resolution, it could only output winter-mean $PM_{2.5}$
323 concentration. It was meaningful to build monthly models to provide more detailed predictions. In addition, modern weather
324 and climate forecasts were heavily dependent on numerical prediction models. Thus, it is imperative to design and develop
325 numerical models that target at routine seasonal prediction of air pollution (Yin et al., 2021). The theories and methods for
326 seasonal prediction of $PM_{2.5}$ concentration are still exploratory and need further discoveries. Considering the severe impact
327 of haze pollution, real-time climate prediction is highly demanded for the purpose to determine how to reduce anthropogenic
328 emissions and how much should be reduced.

329 **Data availability**

330 The monthly sea ice concentration and sea surface temperature (SST) dataset were provided by the Met Office Hadley
331 Centre: <https://www.metoffice.gov.uk/hadobs/hadisst/> (Rayner et al. 2003). Monthly soil moisture, snow depth, geopotential
332 height at 500hPa and 850hPa, sea level pressure and 10m wind were extracted from the fifth generation reanalysis product
333 (ERA5) produced by the European Center for Medium Range Weather Forecasts:
334 <https://cds.climate.copernicus.eu#!/search?text=ERA5&type=dataset> (Hersbach et al. 2020). Annual emissions of ammonia,
335 nitrogen oxide, BOC, primary $PM_{2.5}$, and sulfur dioxide in China were derived from the MEIC model:
336 <http://www.meicmodel.org/> (Li et al., 2017). Hourly site-observed $PM_{2.5}$ concentration during 2014–2020 were acquired
337 from the China National Environmental Monitoring Centre: <https://www.aqistudy.cn/historydata/> (CNEMC, 2021). The
338 long-term and high-resolution TAP $PM_{2.5}$ concentration dataset during 2000-2020 can be downloaded from <http://tapdata.org>
339 (Geng et al. 2021b).

340 **Authors' contribution**

341 Wang H. J. and Yin Z. C. designed this research. Li Y. Y., Xu T. B. and Duan M. K. performed analyses and trained
342 prediction models. Yin Z. C. prepared the manuscript with contributions from all co-authors.

343 **Competing interests**

344 The authors declare no conflict of interest.

345 **Acknowledgements**

346 This research is supported by the National Natural Science Foundation of China (No. 42088101).



347 **References**

- 348 An, J., Chen, Y., Qu, Y., Chen, Q., Zhuang, B., Zhang, P., and Wu, Q.: An online-coupled unified air quality forecasting
349 model system, China, *Adv. Earth Sci.*, 33, 445–454, <https://doi.org/10.11867/j.issn.1001-8166.2018.05.0445>, 2018.
- 350 Chang, L., Wu, Z., and Xu, J.: Contribution of Northeastern Asian stratospheric warming to subseasonal prediction of the
351 early winter haze pollution in Sichuan Basin, China, *Sci Total Environ*, 751, 141823,
352 <https://doi.org/10.1016/j.scitotenv.2020.141823>, 2021.
- 353 Cheng, X. G., Boiyo, R., Zhao, T. L., Xu, X. D., Gong, S. L., Xie, X. N., and Shang, K.: Climate modulation of Niño3.4
354 SST-anomalies on air quality change in southern China: Application to seasonal forecast of haze pollution, *Atmos. Res.*, 225,
355 157–164, <https://doi.org/10.1016/j.atmosres.2019.04.002>, 2019.
- 356 Cohen, A. J., Brauer, M., Burnett, R., Anderson, H. R., Frostad, J., Estep, K., Balakrishnan, K., Brunekreef, B., Dandona, L.,
357 Dandona, R., Feigin, V., Freedman, G., Hubbell, B., Jobling, A., Kan, H., Knibbs, L., Liu, Y., Martin, R., Morawska, L.,
358 Pope, C. A., Shin, H., Straif, K., Shaddick, G., Thomas, M., van Dingenen, R., van Donkelaar, A., Vos, T., Murray, C. J. L.,
359 and Forouzanfar, M. H.: Estimates and 25-year trends of the global burden of disease attributable to ambient air pollution: an
360 analysis of data from the Global Burden of Diseases Study 2015, *The Lancet*, 389, 1907–1918,
361 [https://doi.org/10.1016/s0140-6736\(17\)30505-6](https://doi.org/10.1016/s0140-6736(17)30505-6), 2017.
- 362 Dong, Y., Yin, Z. C., and Duan, M. K.: Seasonal prediction of winter haze days in the Yangtze River Delta, China,
363 *Transactions of Atmospheric Sciences*, 44, 290–301, <https://doi.org/10.13878/j.cnki.dqkxxb.20200525001>, 2021.
- 364 Dun, M., Xu, Z., Wu, L., and Yang, Y.: Predict the particulate matter concentrations in 128 cities of China, *Air. Qual. Atmos.*
365 *Hlth.*, 13, 399–407, <https://doi.org/10.1007/s11869-020-00819-5>, 2020.
- 366 Gao, M., Sherman, P., Song, S., Yu, Y., Wu, Z., and McElroy, M. B.: Seasonal prediction of Indian wintertime aerosol
367 pollution using the ocean memory effect, *Science Advances*, 5, eaav4157, <https://doi.org/10.1126/sciadv.aav4157>, 2019.
- 368 Geng, G., Zheng, Y., Zhang, Q., Xue, T., Zhao, H., Tong, D., Zheng, B., Li, M., Liu, F., Hong, C., He, K., and Davis, S. J.:
369 Drivers of PM_{2.5} air pollution deaths in China 2002–2017, *Nat. Geosci.*, 14, 645–650, [https://doi.org/10.1038/s41561-021-](https://doi.org/10.1038/s41561-021-00792-3)
370 [00792-3](https://doi.org/10.1038/s41561-021-00792-3), 2021a.
- 371 Geng, G., Xiao, Q., Liu, S., Liu, X., Cheng, J., Zheng, Y., Xue, T., Tong, D., Zheng, B., Peng, Y., Huang, X., He, K., and
372 Zhang, Q.: Tracking Air Pollution in China: Near Real-Time PM_{2.5} Retrievals from Multisource Data Fusion, *Environ. Sci.*
373 *Technol.*, 55, <https://doi.org/12106-12115>, [10.1021/acs.est.1c01863](https://doi.org/10.1021/acs.est.1c01863), 2021b.
- 374 He, C., Liu, R., Wang, X. M., Liu, S. C., Zhou, T. J., and Liao, W. H.: How does El Nino-Southern Oscillation modulate the
375 interannual variability of winter haze days over eastern China?, *Sci. Total. Environ.*, 651, 1892–1902,
376 <https://doi.org/10.1016/j.scitotenv.2018.10.100>, 2019.



- 377 Hersbach, H., Bell, B., Berrisford, P., Hirahara, S., Horányi, A., Muñoz-Sabater, J., Nicolas, J., Peubey, C., Radu, R.,
378 Schepers, D., Simmons, A., Soci, C., Abdalla, S., Abellan, X., Balsamo, G., Bechtold, P., Biavati, G., Bidlot, J., Bonavita,
379 M., Chiara, G., Dahlgren, P., Dee, D., Diamantakis, M., Dragani, R., Flemming, J., Forbes, R., Fuentes, M., Geer, A.,
380 Haimberger, L., Healy, S., Hogan, R. J., Hólm, E., Janisková, M., Keeley, S., Laloyaux, P., Lopez, P., Lupu, C., Radnoti, G.,
381 Rosnay, P., Rozum, I., Vamborg, F., Villaume, S., and Thépaut, J. N.: The ERA5 global reanalysis, *Q. J. Roy. Meteor. Soc.*,
382 146, 1999–2049, <https://doi.org/10.1002/qj.3803>, 2020.
- 383 Hsu, P.-c., Zang, Y., Zhu, Z., and Li, T.: Subseasonal-to-seasonal(S2S) prediction using the spatial-temporal projection model
384 (STPM), China, *Transactions of Atmospheric Sciences*, 43, 212–224, <https://doi.org/10.13878/j.cnki.dqkxxb.20191028002>,
385 2020.
- 386 Huang, Y. Y., Wang, H. J., Zhang, P. Y.: A skillful method for precipitation prediction over eastern China, *Atmospheric and*
387 *Oceanic Science Letters*, 15 (1): 100133, <https://doi.org/10.1016/j.aosl.2021.100133>, 2022.
- 388 Li, M., Liu, H., Geng, G., Hong, C., Liu, F., Song, Y., Tong, D., Zheng, B., Cui, H., Man, H., Zhang, Q., and He, K.:
389 Anthropogenic emission inventories in China: a review, *Natl. Sci. Rev.*, 4, 834–866, <https://doi.org/10.1093/nsr/nwx150>,
390 2017.
- 391 Rayner, N. A., Parker, D. E., Horton, E. B., Folland, C. K., Alexander, L. V., Rowell, D. P., Kent, E. C., and Kaplan, A.:
392 Global analyses of sea surface temperature, sea ice, and night marine air temperature since the late nineteenth century. *J.*
393 *Geophys. Res.*, 108, 4407, <https://doi.org/10.1029/2002JD002670>, 2003.
- 394 Wang, H. J., Chen, H. P., and Liu, J. P.: Arctic sea ice decline intensified haze pollution in eastern China, *Atmospheric and*
395 *Oceanic Science Letters*, 8, 1–9, <https://doi.org/10.3878/AOSL20140081>, 2015.
- 396 Wang, H., Dai, Y., Yang, S., Li, T., Luo, J., Sun, B., Duan, M., Ma, J., Yin, Z., and Huang, Y.: Predicting climate anomalies:
397 A real challenge, *Atmospheric and Oceanic Science Letters*, <https://doi.org/100115>, 10.1016/j.aosl.2021.100115, 2021.
- 398 Wang, J. and Du, P.: Quarterly PM_{2.5} prediction using a novel seasonal grey model and its further application in health
399 effects and economic loss assessment: evidences from Shanghai and Tianjin, China, *Nat. Hazards*, 107, 889–909,
400 <https://doi.org/10.1007/s11069-021-04614-y>, 2021.
- 401 Wang, H., Sun, J., Lang, X.: Some New Results in the Research of the Interannual Climate Variability and Short-Term
402 Climate Prediction, China, *Chinese Journal of Atmospheric Sciences*, 32, 806–814, 2008.
- 403 World Health Organization: global air quality guidelines: particulate matter (PM_{2.5} and PM₁₀), ozone, nitrogen dioxide,
404 sulfur dioxide and carbon monoxide, <https://apps.who.int/iris/handle/10665/345329>, 2021.
- 405 Wu, J., Shi, Y., Asweto, C. O., Feng, L., Yang, X., Zhang, Y., Hu, H., Duan, J., and Sun, Z.: Fine particle matters induce
406 DNA damage and G₂/M cell cycle arrest in human bronchial epithelial BEAS-2B cells, *Environ Sci Pollut Res Int*, 24,



- 407 25071-25081, <https://doi.org/10.1007/s11356-017-0090-3>, 2017.
- 408 Wu, L. F., Li, N., and Zhao, T.: Using the seasonal FGM(1,1) model to predict the air quality indicators in Xingtai and
409 Handan, *Environ Sci Pollut Res Int*, 26, 14683-14688, <https://doi.org/10.1007/s11356-019-04715-z>, 2019.
- 410 Xiao, Q., Zheng, Y., Geng, G., Chen, C., Huang, X., Che, H., Zhang, X., He, K., and Zhang, Q.: Separating emission and
411 meteorological contributions to long-term PM_{2.5} trends over eastern China during 2000–2018, *Atmos. Chem. Phys.*, 21,
412 9475-9496, <https://doi.org/10.5194/acp-21-9475-2021>, 2021.
- 413 Xiong, P., Yan, W., Wang, G., and Pei, L.: Grey extended prediction model based on IRLS and its application on smog
414 pollution, *Appl. Soft Comput.*, 80, 797-809, <https://doi.org/10.1016/j.asoc.2019.04.035>, 2019.
- 415 Xu, X., Zhao, T., Liu, F., Gong, S. L., Kristovich, D., Lu, C., Guo, Y., Cheng, X., Wang, Y., and Ding, G.: Climate
416 modulation of the Tibetan Plateau on haze in China, *Atmos. Chem. Phys.*, 16, 1365-1375, [https://doi.org/10.5194/acp-16-](https://doi.org/10.5194/acp-16-1365-2016)
417 1365-2016, 2016.
- 418 Yin, Z. C. and Wang, H. J.: Seasonal prediction of winter haze days in the north central North China Plain, *Atmos. Chem.*
419 *Phys.*, 16, 14843–14852, <https://doi.org/10.5194/acp-16-14843-2016>, 2016.
- 420 Yin, Z. C. and Wang, H. J.: Statistical Prediction of Winter Haze Days in the North China Plain Using the Generalized
421 Additive Model, *J. Appl. Meteorol. Clim.*, 56, 2411–2419, <https://doi.org/10.1175/jamc-d-17-0013.1>, 2017.
- 422 Yin, Z. C. and Wang, H. J.: The relationship between the subtropical Western Pacific SST and haze over North-Central North
423 China Plain, *Int. J. Climatol.*, 36, 3479-3491, <https://doi.org/10.1002/joc.4570>, 2016.
- 424 Yin, Z. C. and Wang, H. J.: The strengthening relationship between Eurasian snow cover and December haze days in central
425 North China after the mid-1990s, *Atmos. Chem. Phys.*, 18, 4753–4763, <https://doi.org/10.5194/acp-18-4753-2018>, 2018.
- 426 Yin, Z. C. and Zhang, Y. J.: Climate anomalies contributed to the rebound of PM_{2.5} in winter 2018 under intensified regional
427 air pollution preventions, *Sci Total Environ*, 726, 138514, <https://doi.org/10.1016/j.scitotenv.2020.138514>, 2020a.
- 428 Yin, Z. C., Li, Y. Y., and Wang, H. J.: Response of early winter haze in the North China Plain to autumn Beaufort sea ice,
429 *Atmos. Chem. Phys.*, 19, 1439–1453, <https://doi.org/10.5194/acp-19-1439-2019>, 2019.
- 430 Yin, Z. C., Wang, H. J., Liao, H., Fan, K., and Zhou, B. T.: Seasonal to interannual prediction of air pollution in China:
431 Review and insight, *Atmospheric and Oceanic Science Letters*, 100131, <https://doi.org/10.1016/j.aosl.2021.100131>, 2022.
- 432 Yin, Z. C., Wang, H. J., and Guo, W. L.: Climatic change features of fog and haze in winter over North China and Huang-
433 Huai Area, China, *Sci. China Earth Sci.*, 58, 1370–1376, <https://doi.org/10.1007/s11430-015-5089-3>, 2015.
- 434 Yin, Z. C., Zhang, Y. J., Wang, H. J., and Li, Y. Y.: Evident PM_{2.5} drops in the east of China due to the COVID-19
435 quarantine measures in February, *Atmos. Chem. Phys.*, 21, 1581–1592, <https://doi.org/10.5194/acp-21-1581-2021>, 2021.



- 436 Yin, Z. C., Zhou, B. T., Chen, H. P., and Li, Y. Y.: Synergetic impacts of precursory climate drivers on interannual-decadal
437 variations in haze pollution in North China: A review, *Sci. Total Environ.*, 755, 143017,
438 <https://doi.org/10.1016/j.scitotenv.2020.143017>, 2020b.
- 439 Zhang, Q., Yin, Z. C., Xi, L., and co-authors.: Synergistic Roadmap of Carbon Neutrality and Clean Air for China 2021,
440 *Environmental Science and Ecotechnology*, Under Review, 2022.
- 441 Zhang, Q. and Geng, G. N.: Impact of clean air action on PM_{2.5} pollution in China, *Sci. China Earth Sci.*, 62, 1845–1846,
442 <https://doi.org/10.1007/s11430-019-9531-4>, 2020.
- 443 Zhao, Z., Liu, S. C., Liu, R., Zhang, Z., Li, Y., Mo, H., Wu, Y.: Contribution of climate/meteorology to winter haze pollution
444 in the Fenwei Plain, China, *Int. J. Climatol.*, 41, 4987-5002. <https://doi.org/10.1002/joc.7112>, 2021.
- 445 Zou, Y. F., Wang, Y. H., Zhang, Y. Z., and Koo, J.-H.: Arctic sea ice, Eurasia snow, and extreme winter haze in China,
446 *Science Advances*, 3, e1602751, <https://doi.org/10.1126/sciadv.1602751>, 2017.